Journal of Materials Chemistry C

Accepted Manuscript

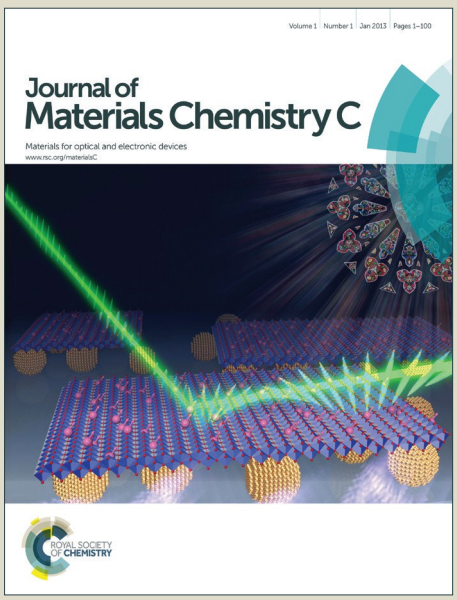

ROYAL SOCIETY OF CHEMISTRY

www.rsc.org/materialsC

Journal of
Materials Chemistry C

PAPER

View Article Online
View Journal

Cite this: DOI: 10.1039/xoxxoooooox

Surfactant Effect on and Luminescence Tuning of Lanthanide-Doped $ScPO_4 \cdot 2H_2O$ Microparticles

Received ooth August 2015,
Accepted ooth August 2015

DOI: 10.1039/xoxxoooooox

www.rsc.org/

Hongjin Chang[a], Yongsheng Zhu[c], Juan Xie[b], Hongyu Li[a], Botong Liu[a], Shuilin Xu[a], Xiaoji Xie[a,*], Ling Huang[a,*] and Wei Huang[a,b,*]

Herein we report the effect of surfactant molecules, i.e., trisodium citrate, on the morphology, size evolution, as well as the growth mechanism of $ScPO_4 \cdot 2H_2O$:Ln (Ln = Ce/Tb/Eu, Yb/Er) microparticles, which were synthesized via one-pot hydrothermal method. The up- and downconversion photoluminescence and dynamics of $ScPO_4 \cdot 2H_2O$:Ln microparticles, including the decay time, quantum efficiency, and the energy transfer mechanism with different dopants were further investigated. Finally, a potential application of these materials as luminescent display inks was demonstrated.

Introduction

Lanthanide-doped luminescent materials have drawn increased attention in the past decades due to their unique optical properties including but not limited to tunable luminescence, high optical stability, and large anti-Stokes shift,[1-11] which exhibit great promise in the areas ranging from biolabeling, biosensing, lasing, photovoltaics, lighting, and phosphors.[12-21] Among these luminescent materials, Sm^{3+}, Eu^{3+}, Dy^{3+}, Tb^{3+}, and Er^{3+} doped lanthanide phosphates ($LnPO_4$) are particularly attractive as commercial phosphors.

To synthesize $LnPO_4$ with desired properties, it is critical to understand clearly the role of surfactant molecules, which help to achieve the proper control of synthesis, in terms of morphology, sizes, and even the crystal structures.[22] In recent years, various efforts have been devoted to the controlled synthesis of various $LnPO_4$ nano/microparticles via the assistance of according surfactant molecules.[23-28] Typically, the wet-chemical route such as hydrothermal synthesis is employed for $LnPO_4$ synthesis due to its versatility, easy operation, and high adjustability.[29,30] For example, luminescent $LnPO_4$ spheres have been synthesized with different morphology by adjusting the pH value of the reaction mixture, surfactant, and the reaction temperature.[31] Controlled synthesis of $LnPO_4$ enables deep understanding of these luminescent materials, in terms of both the crystal growth process and the optical properties at various morphologies, where surfactant molecules are at unparalleled importance. The luminescent properties of these spheres are usually tuned by proper control of the lanthanide dopants.[32] For example, codoping of Ce^{3+} is employed to enhance the emission of Tb^{3+} or Eu^{3+}, via energy transfer from the excited 5d energy level of Ce^{3+} to that of the 4f level of Tb^{3+} or Eu^{3+}.[27]

Despite the advances on $LnPO_4$ studies, Scandium (Sc)-based luminescent materials have so far received very little attention.[33-36] Sc owns the smallest ionic radius and distinct electron configuration among the rare earth family. Importantly, Sc shows distinct features in alloy and optical materials compared with other lanthanide elements. For example, the addition of small amount of Sc would largely enhance the lifetime and intensity of the luminescence of the according materials.[37]

However, there is not very much report on lanthanide-doped $ScPO_4$ microparticles, such as the synthesis conditions, the crystal structure and growth process, as well as the luminescent properties, especially what would be the difference when compared with other rare earth-based phosphates. In this work, by controlling the amount of surfactant, herein, sodium citrate, the growth mechanism and luminescent properties of $ScPO_4 \cdot 2H_2O$:Ln (Ln = Ce/Tb/Eu, Yb/Er) microparticles are investigated. Furthermore, by a simple annealing process, the $ScPO_4 \cdot 2H_2O$ microparticles can be converted to $ScPO_4$

[a]*Key Laboratory of Flexible Electronics (KLOFE) & Institute of Advanced Materials (IAM), Jiangsu National Synergistic Innovation Center for Advanced Materials (SICAM), Nanjing Tech University (NanjingTech), 30 South Puzhu Road, Nanjing 211816, P.R. China*
[b]*Key Laboratory for Organic Electronics and Information Displays & Institute of Advanced Materials (IAM), Jiangsu National Synergistic Innovation Center for Advanced Materials (SICAM), Nanjing University of Posts & Telecommunications, 9 Wenyuan Road, Nanjing 210023, China.*
[c]*Physics and Electronic Engineering College, Nanyang Normal Univerity, Nanyang 473061, China*

without obvious morphology change, but with enhanced luminescence. Finally, the application of $ScPO_4{\cdot}2H_2O$:Ce/Tb/Eu microparticles as display materials has been proofed.

Results and discussion

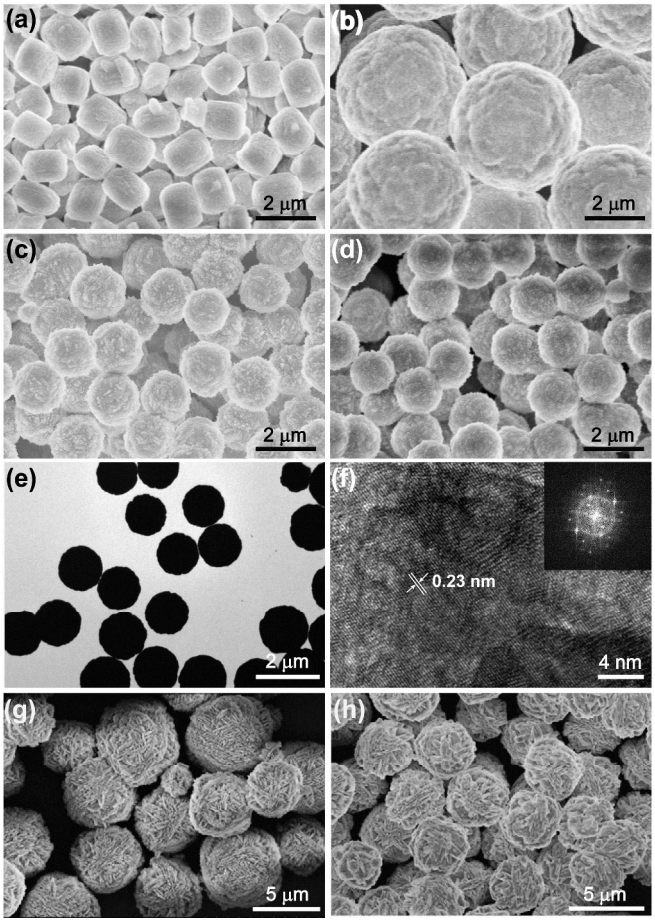

Fig. 1 (a-d) SEM images of $ScPO_4{\cdot}2H_2O$ microparticles synthesized at the Cit^{3-}:Sc^{3+} molar ratio of: (a) 0:1, (b) 1:1, (c) 2:1, and (d) 3:1. (e, f) TEM and HRTEM images of samples in (c). The inset in (f) is the Fourier transform diffraction pattern of the HRTEM image. (g-h) SEM images of the $ScPO_4{\cdot}2H_2O$ microspheres obtained at the PO_4^{3-}:Sc^{3+} molar ratios of: (g) 2:1, (h) 3:1. All the $ScPO_4{\cdot}2H_2O$ microparticles were prepared at 180 °C for 24 h.

Fig. 1 shows SEM and TEM images of $ScPO_4{\cdot}2H_2O$ microparticles synthesized at varying amount of surfactant molecules. At the absence of Cit^{3-}, the product is cubic particles with average dimension of ~0.8×1.6 μm (Fig. 1a). When the molar ratio of Cit^{3-}:Sc^{3+} is 1, spherical microparticles (Fig. 1b) with diameter of ~4.4 μm were obtained. Increase of the Cit^{3-}:Sc^{3+} molar ratio would further reduce the size of the microparticles to ~1.4 μm (Figs. 1c and 1d). However, the size and morphology of the product do not change significantly when the molar ratio of Cit^{3-}:Sc^{3+} is larger than 2. The XRD data (Fig. S1a) confirms that the amount of Cit^{3-} used would not affect the formation of pure monoclinic $ScPO_4{\cdot}2H_2O$ microparticles, which corresponds well with the characteristic monoclinic crystal lattice constant of 0.23 nm in the TEM images (Figs. 1e and 1f).

On the other side, TEM images in Figs. 1g and 1h indicate that the size and morphology of the microparticles are also affected by the molar ratio of Sc^{3+}:PO_4^{3-} (i.e., the amount of PO_4^{3-} used), which provides another possibility for the product adjustment.

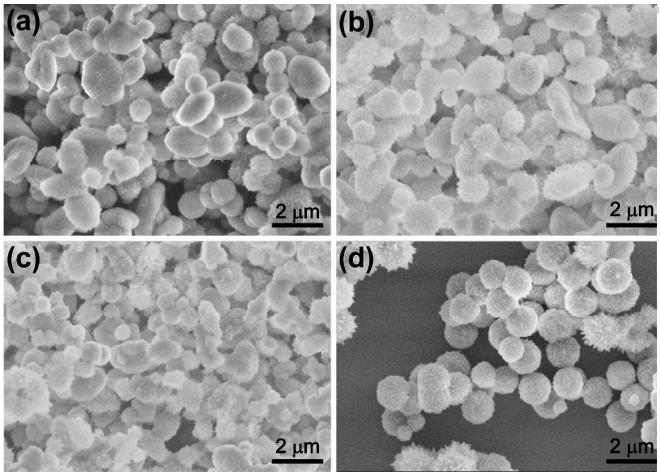

Fig. 2 SEM images of $ScPO_4{\cdot}2H_2O$ microparticles synthesized at 180 °C for (a) 1 h, (b) 3 h, (c) 5 h, and (d) 12 h. The molar ratio of Cit^{3-}:Sc^{3+} was 2:1.

To further understand the growth process of $ScPO_4{\cdot}2H_2O$ microparticles, a series of time-dependent experiments are carried out, during which the reaction temperature and the molar ratio of Cit^{3-}:Sc^{3+} remain unchanged (i.e., 180 °C, Cit^{3-}:Sc^{3+} = 2:1). Result in Fig. 2a indicates that even at the reaction time of 1 h, $ScPO_4{\cdot}2H_2O$ particles at the monoclinic phase can be formed, but with large variation on morphology (from spheres to ellipsoids) and size (from ~0.5 μm to ~2.0 μm), and the products remain similar when the reaction time is increased to 3 h (Fig. 2b) and 5 h (Fig. 2c), respectively. However, regular spheres with small size variation becomes the main product at the reaction time of 12 h, and after 24 h reaction, microparticles with diameter of ~1.4 μm become the only product (Fig. 1c). XRD data (Fig. S1b) also prove that all the products are at pure monoclinic phase, which can be formed even at the reaction time of 1 h, and then the small crystals gradually merge together into large microparticles when the reaction time increases.

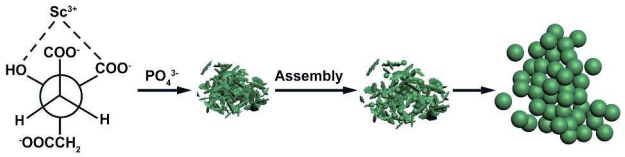

Fig. 3 Schematic illustration of the growth process of $ScPO_4{\cdot}2H_2O$ microparticles.

Based on the above scenario, a reaction scheme is proposed in Fig. 3 to illustrate the growth process of the $ScPO_4{\cdot}2H_2O$ microparticles. It should be noted that, in this hydrothermal synthesis system, Cit^{3-} has two important roles: 1) as surfactant molecule that controls the morphology of the crystals because of its different binding energy at

each crystal facets,[38] and 2) to control the growth rate of the $ScPO_4$ crystals,[39] where Cit^{3-} first forms complex with Sc^{3+}, then the latterly-added PO_4^{3-} will compete with Cit^{3-} to form $ScPO_4$ precipitates. So the crystal growth rate would be related with the releasing rate of the Sc^{3+} in this reaction system. Since it is almost a random assembly of the small crystals at the very beginning of the reaction, large variation on morphology and size were observed. After the Ostwald ripening process at increased reaction time, small crystals are depleted and large spheres are formed via the self-assembly process.[23] The SEM images in Figs. 2a-2d provided a glimpse of the products generated at each intermediate state.

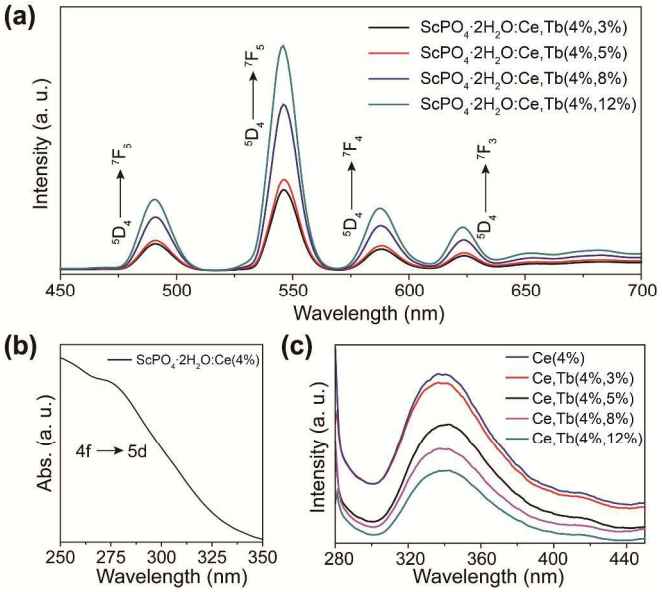

Fig. 4 (a) Room temperature emission of $ScPO_4{\cdot}2H_2O$:Ce,Tb microparticles at different Tb^{3+} doping concentration under 260 nm excitation. (b) UV-vis absorption spectrum of $ScPO_4{\cdot}2H_2O$ microparticles doped with 4% Ce^{3+}. (c) Emission spectra of Ce^{3+} in $ScPO_4{\cdot}2H_2O$ microparticles co-doped with varying Tb^{3+} concentration under 260 nm excitation.

In terms of the luminescent properties, $ScPO_4{\cdot}2H_2O$:Tb microparticles give weak emission under UV excitation due to the low luminescence efficiency.[40] To enhance the luminescence, Ce^{3+} was co-doped with Tb^{3+} into the host material and the intensity of the characteristic emission of Tb^{3+} keeps increasing at increased Tb^{3+} doping concentration (Fig. 4a). The four emission peaks can be attributed to the transitions between the excited $^5D_4$ state and the ^7F_J (J = 6, 5, 4, 3) ground states of Tb^{3+}. Notably, Ce^{3+} here is used as a sensitizer due to the parity allowed 4f-5d transition and its large absorption cross-section at ultraviolet range. Benefited from the efficient energy transfer from Ce^{3+} to Tb^{3+}, enhancement of Tb^{3+} emission is realized.

To understand the energy transfer process between Ce^{3+} and Tb^{3+}, the optical properties of Ce^{3+} under UV excitation is characterized. As shown in Fig. 4b, the Ce^{3+} doped $ScPO_4{\cdot}2H_2O$ microparticles exhibit a typical absorption of the transition between its 4f and 5d states at ~275 nm. When excited under UV light, a broad band emission with maximum at ~340 nm is observed (Fig. 4c), which can be assigned to the energy transition from the 2d state to the ground $^2F_{7/2}$ state of Ce^{3+}.[41] As anticipated, the Ce^{3+} emission gradually decreases with the increase of the doped Tb^{3+} concentration (Fig. 4c), which is very obvious because, the more Tb^{3+} are doped into the crystal lattice (below the quench concentration), the more efficient the energy transfer between Ce^{3+} and Tb^{3+} will be, and the weaker the intensity of the Ce^{3+} emission will become. To achieve multicolor luminescence emission, $ScPO_4{\cdot}2H_2O$:Ce/Eu microparticles with typical luminescence emission at ~620 nm of Eu^{3+} has been synthesized under the same reaction conditions (Fig. S2).

Further study of the decay curves of Tb^{3+} emission at ~550 nm shows a nearly millisecond lifetime (Fig. S3), which confirms the f-f transition of Tb^{3+}.[27a] The lifetime of Tb^{3+} emission at ~550 nm decreases at increased doping concentration of Tb^{3+}, which is due to the conventional cross relaxation between Tb^{3+} at high doping concentration.[42] The measured external quantum yield of $ScPO_4$:Ce/Tb (4%,12%) microparticles is about 27% despite the existence of H_2O molecules.

Based on the above discussion, a scheme depicting the energy transfer process of the Ce^{3+},Tb^{3+} (or Ce^{3+},Eu^{3+}) co-doped $ScPO_4{\cdot}2H_2O$ microparticles is depicted in Fig. S4.[27a] Upon UV excitation, the Ce^{3+} is excited from its $^2F_{5/2}$ to 5d state, the energy is then transferred from the 5d state (300 nm to 450 nm) of the Ce^{3+} to the high excitation levels of Tb^{3+} (or Eu^{3+}) followed by cross relaxation. Subsequently, the Tb^{3+} (or Eu^{3+}) gives its characteristic emissions and returns to the ground state.

Pure $ScPO_4$:Ce,Tb,Eu microparticles are obtained by annealing $ScPO_4{\cdot}2H_2O$:Ce,Tb,Eu(4%,4%,4%) microparticles at 800 °C in N_2 atmosphere, where the monoclinic crystal structure is changed to tetragonal (Fig. S5). The thermogravimetric plot shows that the complete H_2O loss starts at ~300 °C (Fig. S6a), and sequentially the enhanced luminescence is seen (Fig. S6b), which is due to the removal of the OH^- group.[43]

The energy upconversion behavior of the $ScPO_4{\cdot}2H_2O$:Yb/Er microparticles before and after annealing at 800 °C for 3 h is further investigated. Under 980 nm NIR excitation, the annealed sample gives stronger emission when compared with its H_2O containing counterpart (Fig. S7). The green emission at 528 nm and 553 nm originates from the energy transition from $^2H_{11/2}$ to $^4I_{15/2}$ and $^4S_{3/2}$ to $^4I_{15/2}$, while the weak red emission at 660 nm corresponds to the $^4F_{9/2}$ to $^4I_{15/2}$ transition.[44] Considering the efficient energy transfer from exited Er^{3+} and Yb^{3+} to water molecules, we reason that the upconversion emission enhancement attributed to the removal of the coordination water molecules.[45] These results indicate that $ScPO_4$:Yb/Er can work as a good host for UC luminescence.

To shed light on the applications, aqueous solution of $ScPO_4{\cdot}2H_2O$:Ce,Tb(4%,12%) and $ScPO_4{\cdot}2H_2O$:Ce,Eu(4%,12%) microparticles are used as a proof-of-concept luminescent ink for color display. The letters of 'IAM' on the glass substrate are patterned using $ScPO_4{\cdot}2H_2O$:Ce,Tb(4%,12%) as the green ink and $ScPO_4{\cdot}2H_2O$:Ce,Eu(4%,12%) as red ink (Fig. 5). The substrate gives strong luminescence under UV irradiation, while no luminescence is

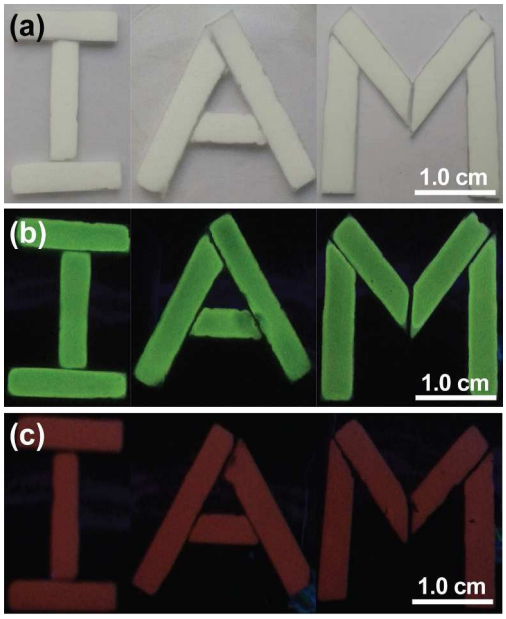

Fig. 5 Images of $ScPO_4{\cdot}2H_2O$:Ce,Tb(4%,12%) luminescent ink patterned on glass substrate under excitation of (a) day light, (b) UV light, and (c) $ScPO_4{\cdot}2H_2O$:Ce,Eu(4%,12%) under UV light.

observed under the daylight irradiation, which indicates that $ScPO_4{\cdot}2H_2O$:Ce/Tb/(Eu) microparticles could potentially be used as luminescent materials in lighting, new generation display, and labeling.

Conclusions

In summary, controlled synthesis of $ScPO_4{\cdot}2H_2O$ microparticles has been demonstrated through hydrothermal method. By adjusting the amount of either surfactant or the reactants, $ScPO_4{\cdot}2H_2O$ microspheres, with sizes from ~4 μm to 1 μm can be obtained. The mechanism studies indicate that the microspheres are assembled by small particles in the presence of citrate surfactant. Codoping of Ce^{3+} with Tb^{3+} and Eu^{3+} in the $ScPO_4{\cdot}2H_2O$ microparticles allows the manipulation of their optical properties including the emission wavelengths, intensity, and lifetimes. Additionally, the monoclinic $ScPO_4{\cdot}2H_2O$ microparticles can be transferred into tetragonal $ScPO_4$ microparticles via a simple thermal annealing, which provide a facile method to synthesis $ScPO_4$-based materials. These results should help to enrich the exploration and sequential applications of Sc-based nano/micromaterials in information technology, new generation display, bioimaging, and anti-counterfeit.

Experiment Materials

Scandium chloride ($ScCl_3{\cdot}6H_2O$, 99.9%), Europium chloride ($EuCl_3{\cdot}6H_2O$, 99.9%), Cerium chloride ($CeCl_3{\cdot}6H_2O$, 99.9%), Terbium chloride ($TbCl_3{\cdot}6H_2O$, 99.9%), Ytterbium chloride ($YbCl_3{\cdot}6H_2O$, 99.9%), Erbium chloride ($ErCl_3{\cdot}6H_2O$, 99.9%), Trisodium phosphate (Na_3PO_4), and Trisodium citrate (Na_3Cit) were purchased from Alfa Aesar and used as received unless otherwise noted.

Synthesis

In a typical experiment, 0.3 mmol $ScCl_3{\cdot}6H_2O$ was added into 15 mL aqueous solution containing proper amount of trisodium citrate (Cit^{3-}). After vigorous stirring for 15 min, 0.3 mmol of Na_3PO_4 was added, and the pH of the mixture was adjusted to 2.0 by HCl (3 M). The resulting mixture was transferred into a Teflon-lined stainless steel autoclave (25 mL) and maintained at 180 °C for 24 h. When the autoclave was naturally cooled down to room temperature, the products were washed with water and ethanol several times, dried in air at 80 °C for 24 h and stored for further use. For Eu^{3+}, Tb^{3+}, and Ce^{3+} doped $ScPO_4{\cdot}2H_2O$, the microparticles were prepared following the same procedure. All the doping concentrations were mol%. Annealing of the products was performed at 800 °C under N_2 protection.

Characterization

The powder X-ray diffraction (XRD) data were recorded on a Shimadzu XD-3A X-ray diffractometer with monochromatized Cu Kα radiation (λ = 1.5406 Å). The morphology and size of the products were characterized by the S4800 (Hitachi) field emission scanning electron microscope (FE-SEM) equipped with an energy-dispersive X-ray spectrometer (EDX). Transmission electron microscopy (TEM) images were taken on JEM-200CX, and high-resolution (HRTEM) images were recorded on the FEI Tecnai G20 with an acceleration voltage of 200 kV. Ultraviolet-visible absorption spectra were collected with a Shimadzu UV-3600 scanning spectrophotometer. The emission spectra were recorded using a Hitachi F-4500 spectrophotometer. The decay curves were measured with a FL920 single-photon spectrometer (Edinburgh) using a nanosecond flash lamp (pulse width: 1 ns; repetition rate: 40 kHz) as excitation source. The quantum yield was measured in a FL 920 spectrometer coupled with an integrating sphere. Thermal analyses (TG/DTA) of the sample were carried out on a Pyris 1 DSC instrument (Perkin Elmer) with a heating rate of 10 °C min^{-1} in N_2 atmosphere.

Author Information

*E-mail:
iamxjxie@njtech.edu.cn (X.X.).
iamlhuang@njtech.edu.cn (L.H).
iamwhuang@njtech.edu.cn (W.H.).

Acknowledgements

We thank the financial support from the National Natural Science Foundation of China (No.: 21301090, 21371095) and the Natural Science Foundation of Jiangsu Province (No.: BK20130923). This project was also supported by the Specially Appointed Professors of the Jiangsu Province.

Notes and references

1. F. Wang, X. Liu, *Chem. Soc. Rev.*, 2009, **38**, 976-989.
2. S. Han, R. Deng, X. Xie, X. Liu, *Angew. Chem. Int. Ed.*, 2014, **53**, 11702-11715.
3. G. Chen, H. Qiu, P. N. Prasad, X. Chen, *Chem. Rev.*, 2014, **114**, 5161-5124.
4. M. Haase, H. Schäfer, *Angew. Chem. Int. Ed.*, 2011, **50**, 5808-5829.
5. X. Xie, N. Gao, R. Deng, Q. Sun, Q. Xu, X. Liu, *J. Am. Chem. Soc.*, 2013, **135**, 12608-12611.
6. Y. Liu, D. Tu, H. Zhu, X. Chen, *Chem. Soc. Rev.*, 2013, **42**, 6924-6958.
7. H. Dong, L.-D. Sun, C.-H. Yan, *Nanoscale*, 2013, **5**, 5703-5714.
8. H. Chang, J. Xie, B. Zhao, B. Liu, S. Xu, N. Ren, X. Xie, L. Huang, W. Huang, *Nanomaterials*, 2015, **5,** 1-25.
9. Y. Huang, F. Rosei, F. Vetrone, *Nanoscale*, 2015, **7**, 5178-5185.
10. F. Vetrone, R. Naccache, V. Mahalingam, C. G. Margan, J. A. Capobianco, *Adv. Funct. Mater.*, 2009, **19**, 2924-2929.
11. Z. Sun, Y. Li, X. Zhang, M. Yao, L. Ma, W. Chen, *J. Nanosci. Nanotechnol.*, 2009, **9**, 6283-6291.
12. S. Zeng, M. Tsang, C. Chan, K. Wong, J. Hao, *Biomaterials,* 2012, **33**, 9232-9238.
13. J. Zhou, Z. Yang, W. Dong, R. Tang, L.-D. Sun, C.-H. Yan, *Biomaterials*, 2011, **32**, 9059-9067.
14. J. Boyer, M. Manseau, J. Murray, F. van Veggel, *Langmuir*, 2010, **26**, 1157-1164.
15. W. Li, J. Wang, J. Ren, X. Qu, *J. Am. Chem. Soc.*, 2014, **136**, 2248-2251.
16. J. Zhao, Z. Lu, Y. Yin, C. McRae, J. Piper, J. Dawes, D. Jin, E. Goldys, *Nanoscale*, 2013, **5**, 944-952.
17. G. Chen, J. Shen, T. Y. Ohulchanskyy, N. J. Patel, A. Kutikov, Z. Li, J. Song, R. Pandey, H. Agren, P. N. Prasad, G. Han, *ACS Nano*, 2012, **6**, 8280-8287.
18. L. Wang, M. Lan, Z. Liu, G. Qin, C. Wu, X. Wang, W. Qin, W. Huang, L. Huang, *J. Mater. Chem. C*, 2013, **1**, 2485-2490.
19. V. Mahalingam, F. Vetrone, R. Naccache, A. Speghini, J. A. Capobianco, *Adv. Mater.*, 2009, **21**, 4025-4028.
20. F. Wang, C. Han, F. Li, *Adv. Mater.*, 2013, **25,** 5287-5303.
21. B. Chen, B. Dong, J. Wang, S. Zhang, L. Xu, W. Yu, H. Song, *Nanoscale*, 2013, **5**, 8541-8549.
22. C. Li, J. Lin, *J. Mater. Chem.*, 2010, **20**, 6831-6847.
23. C. Li, Z. Hou, C. Zhang, P. Yang, G. Li, Z. Xu, Y. Fan, J. Lin, *Chem. Mater.*, 2009, **21**, 4598-4607.
24. R. Yan, X. Sun, X. Wang, Q. Peng, Y. Li, *Chem. -Eur. J.*, 2005, **11**, 2183-2195.
25. Z. Yan, Y.-W. Zhang, L. You, R. Si, C.-H. Yan, *J. Cryst. Growth,* 2004, **262**, 408-414.
26. Y. Fang, A. Xu, R. Song, H. Zhang, L. You, J. Yu, H. Liu, *J. Am. Chem. Soc.*, 2003, **125**, 16025-16034.
27. (a) K. Riwotzki, H. Meyssamy, H. Schnablegger, A. Kornowski, M. Haase, *Angew. Chem. Int. Ed.*, 2001, **40**, 573-576; (b) T. K. Srinivasan, B. S. Panigrahi, N. Suriyamurthy, P. K. Parida, B. Venkatraman, *J. Rare Earth*, 2015, **33**, 20-26.
28. P. Ghosh, A. Kar, A. Patra, *J. Appl. Phys.,* 2010, **108**, 113506.
29. G. Wang, Q. Peng, Y. Li, *Acc. Chem. Res.*, 2011, **44**, 322-332.
30. C. Li, J. Lin, *J. Mater. Chem.*, 2010, **20**, 6831-6847.
31. M. Guan, G. Zhu, T. Shang, Z. Xu, J. Sun, Q. Zhou, *CrystEngComm,* 2012, **14**, 6540-6547.
32. F. Wang, X. Xue, X. Liu, *Angew. Chem. Int. Ed.*, 2008, **47**, 906-909.
33. X. Teng, Y. Zhu, W. Wei, S. Wang, J. Huang, R. Naccache, W. Hu, A. Tok, Y. Han, Q. Zhang, Q. Fan, W. Huang, J. A. Capobianco, L. Huang, *J. Am. Chem. Soc.*, 2012, **134**, 8340-8343.
34. Y. Ding, X. Teng, H. Zhu, L. L. Wang, W. Pei, J. Zhu, L. Huang, W. Huang, *Nanoscale*, 2013, **5**, 11928-11932.
35. X. He, B. Yan, *Cryst. Growth Des*., 2014, **14**, 3257-3263.
36. M. Pang, X. Zhai, J. Feng, S. Song, R. Deng, Z. Wang, S. Yao, X. Ge, H. Zhang, *Dalton Trans.*, 2014, **43**, 10202-10207.
37. Q. Huang, J. Yu, E. Ma, K. Lin, *J. Phys. Chem. C,* 2010, **114**, 4719-4724.
38. L. Wang, Y. Li, *Nano Lett.*, 2006, **6**, 1645-1649.
39. Z. Li, Y. Zhang, *Angew. Chem., Int. Ed.,* 2006, **45**, 7732-7735.
40. N. Hashimoto, Y. Takada, K. Sato, S. Ibuki, *J. Lumin.*, 1991, **48-49**, 893-897.
41. J. Bourcet, F. Fong, *J. Chem. Phys.*, 1974, **60**, 34-39.
42. (a) Y. Ruan, Q. Xiao, W. Luo, R. Li, X. Chen, *Nanotechnology*, 2011, **22,** 275701-275705; (b) N. Li, S. Li, Y. Wang, B. Zhou, Y. Sun, J. Zhou, *J. Rare Earth*, 2014, **32**, 933-937.
43. C. Li, Z. Hou, C. Zhang, P. Yang, G. Li, Z. Hu, Y. Fan, J. Lin, *Chem. Mater.*, 2009, **21**, 4598-4607.
44. G. Yi, H. Lu, S. Zhao, G. Yue, W. Yang, D. Chen, L. Guo**,** *Nano Lett.,* 2004, **4**, 2191-2196.
45. R. Arppe, I. Hyppänen, N. Perälä, R. Peltomaa, M. Kaiser, C. Würth, S. Christ, U. Resch-Genger, M. Schäferling, T. Soukka, *Nanoscale*, 2015, **7**, 11746-11757.

UV-excited luminescent patterns of 'IAM' generated using $ScPO_4 \cdot 2H_2O$:Ce,Tb(4%,12%) and $ScPO_4 \cdot 2H_2O$:Ce,Eu(4%,12%) microparticles as green and red display materials, respectively.